Imperfect Hopf bifurcation in spiral Poiseuille flow

J. Abshagen, M. Heise, J. Langenberg, and G. Pfister
Institute of Experimental and Applied Physics, University of Kiel, 24098 Kiel, Germany
(Received 7 January 2005; revised manuscript received 6 October 2006; published 22 January 2007)

We present the results of an experimental study on the transition to spiral vortices in flow between concentric counter-rotating cylinders in the presence of an axial through-flow, i.e., in spiral Poiseuille flow. The experiments were performed in an apparatus having an aspect ratio $\Gamma=L/d=22.8$ (L axial length, d gap width between cylinders) and end plates enabling an in and outflow of mass. As a result of an applied axial through-flow the "classical" Hopf bifurcation to spiral vortices (SPI) splits up and a primary and secondary branch of down and upstream propagating SPI, respectively, as well as a transient quasiperiodic flow appear. Downstream propagating SPI resulting from the primary supercritical Hopf bifurcation are either convectively or absolutely unstable. The bifurcation structure observed in this open flow experiment is in qualitative agreement with predictions from theory of Hopf bifurcation with broken reflection symmetry [J. D. Crawford and E. Knobloch, Nonlinearity **1**, 617 (1988)] and also in quantitative agreement with results from recent numerical calculations [A. Pinter, M. Lücke, and C. Hoffmann, Phys. Rev. E **67**, 026318 (2003); C. Hoffmann, M. Lücke, and A. Pinter, *ibid.* **69**, 056309 (2004)].

DOI: 10.1103/PhysRevE.75.016309 PACS number(s): 47.20.Ky, 05.45.−a, 02.30.Oz

I. INTRODUCTION

Bifurcations [1] play a crucial role in the organization of complex dynamics and patterns in many spatially extended nonlinear systems, such as, e.g., hydrodynamic flows [2]. Time-dependent spatial patterns often appear in flow systems from a Hopf bifurcation of the basic laminar flow state. Examples arise from binary mixture convection [3], magnetoconvection [4], stratified Taylor-Couette flow [5], and from counter-rotating Taylor-Couette flow [6]. In particular symmetries are crucial in order to determine the solution set close to a bifurcation in a spatially extended nonlinear system. Models of bifurcations in pattern forming systems with one spatial dimension often assume an invariance of a physical system under translations and a reflection symmetry, i.e., an O(2)-symmetry. Under such an assumption the critical eigenvalues at a Hopf bifurcation will typically have double multiplicity and the resulting patterns from the basic state gives rise to two types of periodic solutions hereafter referred to as standing waves and traveling waves. The traveling wave solution is further divided into two different branches of traveling waves propagating in opposite directions.

A. Spiral vortices in Taylor-Couette flow

One of the classical hydrodynamic systems for the study of Hopf bifurcation with O(2)-symmetry is counter-rotating Taylor-Couette flow. This is the flow of a viscous liquid in the gap between two concentric rotating cylinders. Under the assumption of cylinders having an infinite axial length basic laminar Couette flow has an axial translational invariance, reflection symmetry, and azimuthal rotational invariance. The flow is thus invariant under the group $O(2)\times SO(2)$ [7]. On the basis of linear stability analysis of laminar Couette flow, Krueger *et al.* [8] predicted the existence of nonaxisymmetric time-dependent spiral vortices resulting from a Hopf bifurcation for sufficiently counter-rotating cylinders. Spiral vortices have in general the form of traveling waves in the axial direction and of rotating waves in the azimuthal direction.

The existence of spiral vortices has been confirmed experimentally by Snyder [9] and Andereck *et al.* [10] in Taylor-Couette flow with different radius ratios η and aspect ratios Γ (ratio of axial length to gap width), respectively. Further combined numerical and experimental investigations on the primary instability and also on bicritical curves in flow between counter-rotating cylinders have been performed by Langford *et al.* [11] and Tagg *et al.* [12]. Transition to spiral vortices and their behavior in the nonlinear regime have been studied in [13]. Experimental investigations from Langenberg *et al.* [14] revealed an influence of finite axial length on the transition to spiral vortices in accordance with the theory of O(2)-symmetric Hopf bifurcation with broken translational invariance [15].

B. Hopf bifurcation with broken symmetries

Experimental systems never have perfect symmetries. For the applicability of bifurcation models to physical experiments it is therefore crucial to understand the influence of broken symmetries on the structure of the symmetric bifurcation. In theory a broken symmetry is reflected by additional imperfection terms in the normal form giving rise to a different bifurcation structure and new dynamics close to the critical point [16]. For example, due to the finite spatial extent of experimental systems the translational invariance is always broken. The effect of broken translational invariance on O(2)-symmetric Hopf bifurcations has been studied theoretically in [15]. The reflection symmetry of an experimental system can be broken by an additional external field, like an imposed mean flow in a hydrodynamic system. The effect of a broken reflection symmetry on O(2)-symmetric Hopf bifurcation has been studied theoretically in [17–19]. The effect of breaking O(2) to SO(2) introduces imperfection terms to the normal form of O(2)-symmetric Hopf bifurcation. For

the non-degenerate case at linear order the perturbed normal form of an O(2)-symmetric Hopf bifurcation with broken reflection symmetry reads

$$\frac{dz_1}{dt} = (\varepsilon + i\omega)z_1 + (b|z_1|^2 + (a+b)|z_2|^2)z_1 + \mu z_1, \qquad (1)$$

$$\frac{dz_2}{dt} = (\varepsilon + i\omega)z_2 + (b|z_2|^2 + (a+b)|z_1|^2)z_2 - \mu z_2 \qquad (2)$$

for the two complex-valued amplitudes $z_1 = r_1 e^{i\Phi_1}$ and $z_2 = r_2 e^{i\Phi_2}$ of the counter-propagating traveling wave solutions $(\varepsilon, \omega, a, b \in \mathbb{R})$ and with the imperfection parameter $\mu = \mu_r + i\mu_i \in \mathbb{C}$. For $\mu_r \neq 0$ the two traveling wave solutions ($z_{1,2} \neq 0$ and $z_{2,1} = 0$) do not bifurcate simultaneously but appear each from a single Hopf bifurcation at different critical points from the basic state with different wave speeds (for $\mu_i \neq 0$). Standing waves ($z_1 = z_2$) are no longer solutions but quasiperiodic modulated waves arising from a secondary bifurcation of a traveling wave. The nonlinear behavior of the bifurcated solutions can be more complicated, in particular close to degeneracy [17].

C. Spiral Poiseuille flow

As a result of an imposed axial through-flow the character of Taylor-Couette flow changes from a closed to an open flow. The basic flow of a Taylor-Couette system with axial through-flow under the assumption of infinite axial length is a superposition of circular Couette and annular Poiseuille flow, called Couette-Poiseuille flow (CPF). The sensitivity of open flows to external perturbation is associated with absolute and convective instabilities [20] which have also been studied in semifinite and finite open flows [21]. In the convective unstable regime small localized perturbations of the basic laminar flow will grow while propagating along with the flow but decay at any spatial point. In the absolute unstable regime a perturbation will grow at any spatial point. Convective and absolute instabilities have been investigated experimentally [22] and theoretically [23] in the "classical" setup with a stationary outer cylinder. Recent numerical [24] and experimental investigations [25] have shown that convective and absolute instabilities occur also at the onset of spiral vortices in counter-rotating Taylor-Couette flow with axial through-flow, called counter-rotating spiral Poiseuille flow. However, the concept of convective and absolute instabilities originates from linear stability theory and thus does not make predictions on the nonlinear behavior of the spiral solutions.

D. Aim of work

The aim of this work is to investigate the effect of symmetry breaking perturbations due to an additional mean flow on the bifurcation structure and the dynamics of the O(2)-symmetric Hopf bifurcation that occur at the onset of spiral vortices in counter-rotating spiral Poiseuille flow.

II. EXPERIMENTAL SETUP

The spiral Poiseuille flow experiment consists of a viscous fluid confined in the gap between two independently rotating concentric cylinders with an imposed axial mean flow. The temperature of the fluid is thermostatically controlled to (24.00 ± 0.01) °C. As working fluid silicon oil with a kinematic viscosity $\nu = 10.6$ cS at 24 °C is used. The inner cylinder of the apparatus is machined from stainless steel having a radius of $r_i = (12.50 \pm 0.01)$ mm, while the outer cylinder is made from optically polished glass with a radius of $r_o = (25.00 \pm 0.01)$ mm. The flow is confined in axial direction by two end plates having a distance L which defines the axial length of the system. Both end plates are shaped identically at top and bottom in order to ensure reflection symmetry of the experimental apparatus. Geometric parameters are the aspect ratio $\Gamma = L/d$, with gap width $d = r_o - r_i$, and the radius ratio $\eta = r_i/r_o$. The radius ratio is held fixed to $\eta = 0.5$ for all measurements and the axial length of the apparatus is $L = 285$ mm which corresponds to an aspect ratio $\Gamma = 22.8$. As control parameters serve the Reynolds number of the inner (i) and the outer (o) cylinder, $\mathrm{Re}_{i,o} = d r_{i,o} \Omega_{i,o} / \nu$, where $\Omega_{i,o}$ denotes the angular velocity of the inner (i) and the outer (o) cylinder, respectively. We utilize laser Doppler velocimetry (LDV) for measurements of the local flow velocity. All time series are recorded with LDV at the same position in the flow, i.e., at a radial distance of 1.3 mm from the inner cylinder in the axial middle. In addition to that flow visualization measurements are performed in order to distinguish between different flow states due to their spatiotemporal patterns.

The end plates confining the flow at the top and bottom of the cylinder are systematically perforated in order to enable a mass flow in the axial direction. Size and distribution of the small wholes in the end plate are carefully chosen in order to enable an inlet flow profile that is as similar as possible to axisymmetric Poiseuille flow. The end plates are held fixed in the laboratory frame and are designed in a way to avoid the azimuthal velocity component of the axial through-flow at the inlet. The Reynolds number of the axial through-flow is defined by $\mathrm{Re}_D = d\langle v \rangle / \nu$, where $\langle v \rangle$ denotes the mean axial velocity. For all measurements Re_D is said to be positive for an axial through-flow directed upward in the laboratory frame and negative for a through-flow directed downward. Its rate is controlled by a precision valve to a resulting accuracy of $\Delta \mathrm{Re}_D = \pm 0.02$. The redistribution length of an axial Poiseuille flow from an inhomogeneous flow at the inlet depends, of course, on Re_D. However, since only small Re_D (≤ 1.5) are investigated and due to the design of the inlet flow profile at the end plate the inhomogeneous velocity distribution at the inlet redistributes to an axial Poiseuille profile even at small axial distances from the inlet. A typical radial profile of the axial velocity, measured at $\mathrm{Re}_{i,o} = 0$ and $\mathrm{Re}_D = 1.5$ at a distance of 12.5 mm from the inlet, is shown in Fig. 1. We observed a reasonable agreement with the analytical Poiseuille profile even at a small distance from the inlet (for example, one times a gap width). Small deviations from the analytical profile are still present here, but disappear quickly as the flow evolves downstream.

The focus of these investigations is on small perturbations of the reflection symmetry and the axial velocity profile is very similar to axial Poiseuille flow, even in the whole flow domain except very close to the end plates.

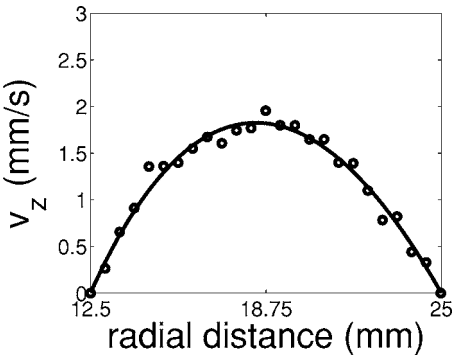

FIG. 1. Radial profile of axial velocity measured at $\mathrm{Re}_{i,o}=0$ at a distance of 12.5 mm (d) above the inflow end plate for $\mathrm{Re}_D=1.5$ (○) in comparison with the analytical Poiseuille profile (solid line).

III. RESULTS

A. Characterization of spiral Poiseuille flow

A recent experimental investigation [14] on length effects in counterrotating Taylor-Couette flow with $\eta=0.5$ has revealed that for an aspect ratio $\Gamma \gtrsim 20$ only counterpropagating spiral vortices but no standing waves appear from a supercritical Hopf bifurcation of the basic flow. Therefore, an aspect ratio $\Gamma=22.8$, which is chosen for our experiments, ensures spiral vortices to appear as the primary pattern for a Hopf bifurcation at least for $\mathrm{Re}_D=0$. At the onset of spiral vortices the flow breaks reflection symmetry and thus two propagating spiral solutions appear. Both flow states are observed in the experiment and are labeled up (SPI↑) and downward propagating spirals (SPI↓) since in laser light sheet measurements of the (r,z) plane vortices seem to propagate either up or downward, respectively, in the laboratory frame. Note that the spiral vortices are not *real* traveling waves like in infinite models but only rotating waves in finite systems. However, since these solutions are related to the propagating solutions in models we will further speak of "propagating spirals". Since SPI↑ and SPI↓ propagate in opposite directions the reflection symmetry of the flow is broken at the Hopf bifurcation. Both values of propagation speed are equal and therefore the oscillation frequencies detected at fixed measurement position by LDV are also identical.

As a result of the axial through-flow the reflection symmetry of a counterrotating Taylor-Couette system is broken. Both flow states (SPI↑ and SPI↓) can also be found in the experiments for supercritical values of Re_i in the case of an applied axial through-flow.

Flow visualizations of both flow states are depicted in Figs. 2(a) and 2(b). Besides their differences in propagation direction spiral vortices can also be distinguished in principle by their azimuthal wave number m which is either +1 or −1. Here, for $\mathrm{Re}_D>0$ and counterclockwise rotating Ω_i upward propagating SPI↑ have an azimuthal wave number $m=+1$ and downward propagating SPI↓ have $m=-1$. In wide-gap counterrotating Taylor-Couette experiments spiral vortices appear only very close to the inner cylinder and are surrounded by a relatively thick layer of nearly laminar Couette and Couette-Poiseuille flow, respectively. This spatial pattern

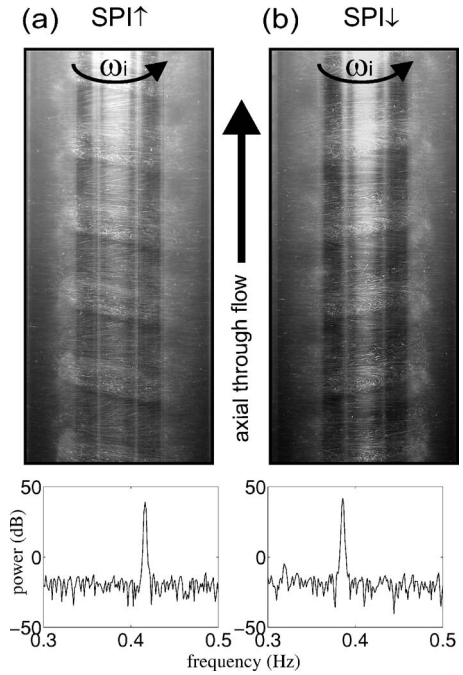

FIG. 2. Flow visualization and power spectra of corresponding time series of up and downward propagating spiral vortices recorded at (a) $\mathrm{Re}_o=-125$, $\mathrm{Re}_D=0.6$, and $\mathrm{Re}_i=125$ for SPI↑ and (b) $\mathrm{Re}_i=133$ for SPI↓.

can be observed in flow visualization as those shown in Fig. 2. In addition to that, laser-light sheet techniques in combination with LDV measurements provide detailed information about spiral vortices at the inner cylinder.

However, since the apparatus is constructed in a way that the external flow can either be directed up- or downward we have to distinguish further between up and downstream propagating spiral vortices, i.e., spirals having a direction of propagating in the opposite or in the same direction as the external flow, respectively. Thus, for example, for $\mathrm{Re}_D>0$, i.e., an imposed flow directed upward, SPI↑ are propagating downstream while SPI↓ are propagating upstream.

Downstream propagating SPI↑ and upstream propagating SPI↓ can be furthermore distinguished due to a frequency shift, that can be detected in power spectra of time series recorded by LDV measurements, towards higher (SPI↑) and lower (SPI↓) oscillation frequencies compared to the frequency at $\mathrm{Re}_D=0$. This frequency shift is a result on the axial through-flow and can be seen in the power spectra of both flow states in Fig. 2.

B. Transition to spirals with axial through-flow

In order to demonstrate the behavior at the transition to spiral vortices in spiral Poiseuille flow an experimental bifurcation diagram is presented in Fig. 3(a). It was measured at $Re_D=-1.5$ (downward directed axial flow) and $\mathrm{Re}_o=-100$. Note that, in order to distinguish SPI↑ and SPI↓ in the same diagram, different measures of the bifurcation for each flow state are chosen. The amplitude of SPI↓ (○) is estimated from the mean of the maxima, whereas the flow state of SPI↑ (◇) is estimated by the minima of the velocity

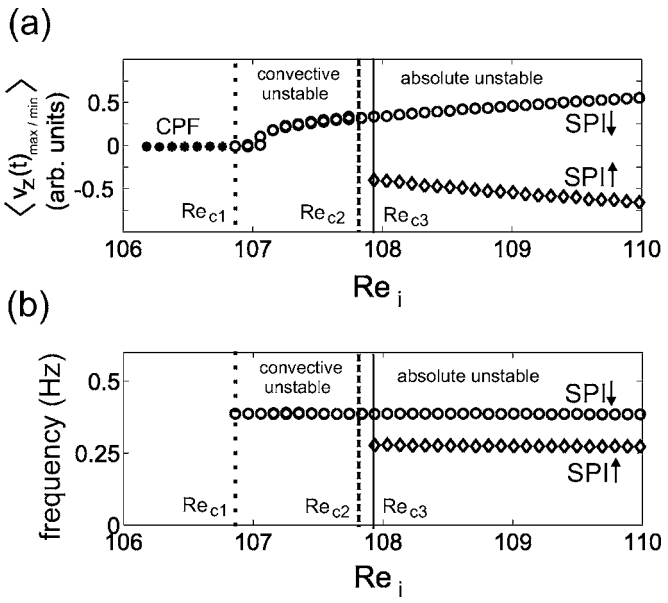

FIG. 3. Bifurcation diagram measured in a spiral Poiseuille flow experiment for $\mathrm{Re}_D=-1.5$ and $\mathrm{Re}_o=-100.0$: (a) Mean of maxima (○) of the axial velocity $v_z(t,L/2)$ is plotted as a measure of the amplitude of SPI↓ and mean of minima (◇) as a measure of the amplitude of SPI↑. Basic flow (●) becomes convectively unstable at Re_{c1} (dotted vertical line), SPI↓ becomes absolutely unstable at Re_{c2} (dashed vertical line), and SPI↑ loses stability at Re_{c3} (solid vertical line). (b) Oscillation frequencies f of SPI↓ (○) and SPI↑ (◇).

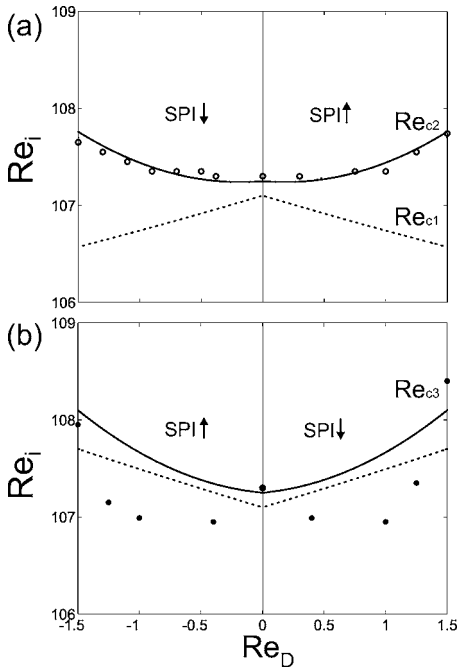

FIG. 4. Stability diagrams of spiral Poiseuille flow for $\mathrm{Re}_o=-100$: (a), (b) Calculated convective (dotted line) and absolute (solid line) linear instability of basic flow with respect to SPI↑ and SPI↓ (linear stability analysis from Pinter *et al.* [24]). (a) Measurements of the absolute instability border (○) of downstream propagating SPI (↓ at $\mathrm{Re}_D<0$ and SPI↑ at $\mathrm{Re}_D>0$) that result from the primary convective instability of the basic flow. (b) Lower instability border (●) of upstream propagating SPI ↑ at $\mathrm{Re}_D<0$ and SPI↓ at $\mathrm{Re}_D>0$.

in the corresponding time series. Starting from the basic laminar flow (denoted as CPF, ●) an increase of Re_i leads to the convective instability border at Re_{c1} and thereby to downstream propagating SPI↓. Note that Fig. 3 represents measurements recorded at $\mathrm{Re}_D=-1.5<0$. Amplitude and phase of SPI↓ are initially fluctuating in the convectively unstable regime. The critical Reynolds number Re_{c1} corresponding to the onset of SPI↓ is defined in the experiment as that Re_i where the characteristic frequency peak of spiral vortices is detectable in power spectrum for the first time. A further increase of Re_i leads to absolutely unstable CPF at Re_{c2}. The threshold is determined in the experiments by the normalized variance of the main peak in the power spectrum

$$\sigma^2 = \frac{\langle (f-\langle f\rangle)^2\rangle}{\langle f\rangle^2}. \tag{3}$$

It is significantly reduced when the flow becomes absolutely unstable (see [25,26] for details). The critical Reynolds numbers have also been determined by linear stability analysis by Pinter *et al.* [24] and show a reasonable agreement with the measurements of the convective and a quantitative agreement for the absolute instability border. An experimental investigation on convective and absolute instability borders of spiral vortices has been performed in [25]. Upstream propagating SPI↑ do not exist below Re_{c3} and cannot be archived by quasistatistical increase of Re_i from subcritical values towards Re_{c3}. But it is possible to observe SPI↑ in the experiment after a sudden increase of Re_i from a value below Re_{c1} towards a value that is larger than Re_{c3}. For these Reynolds numbers SPI↑ is stable and coexists with downstream propagating SPI↓. A decrease of Re_i quasistatically below $\mathrm{Re}_{c3}=107.9$ results in a transition from SPI↑ to SPI↓. Note that, for this particular set of control parameters, Re_{c3} and Re_{c2} have very similar values but it will become evident that they are not identical in general.

In Fig. 3(b) the oscillation frequencies measured from SPI↑ and SPI↓ are depicted. These frequencies have been detected from the power spectra of the corresponding time series as exemplarily depicted in Fig. 2. In this range of Reynolds number the oscillation frequency is almost independent of Re_i for each flow state but a frequency shift between both flow states can be observed. This is a result of the imposed axial through-flow. Downstream propagating SPI↓ have an increased value of oscillation frequency compared to upstream propagating SPI↑.

C. Stability diagram of spiral Poiseuille flow

The stability diagram of spiral Poiseuille flow is depicted in Fig. 4. The convective (dotted) and absolute (solid) instability borders have been calculated by linear stability analysis by Pinter *et al.* [24]. The borders of the convective regime have been verified experimentally for the case of $\mathrm{Re}_D>0$ in [25]. For this case the basic flow becomes convectively unstable towards downstream propagating SPI↑ and SPI↓ for

the case of $\mathrm{Re}_D<0$—dotted line in Fig. 4(a). The basic flow state becomes absolutely unstable to one of these flow states at higher Re_i represented by the solid line in Fig. 4(a). The convective instability border of upstream propagating SPI↑ for $\mathrm{Re}_D<0$ and ↓ for $\mathrm{Re}_D>0$, respectively, is depicted as a dotted line in Fig. 4(b). Note that here the basic Couette-Poiseuille flow is already convectively unstable towards downstream propagating SPI (↑ for $\mathrm{Re}_D<0$ and ↓ for $\mathrm{Re}_D>0$). The Couette-Poiseuille flow becomes absolutely unstable to upstream propagating flow states at higher Re_i represented by the solid line in Fig. 4(b).

In the experiments we observe that by a quasistatistical increase of Re_i from subcritical values downstream propagating SPI (↓ for $\mathrm{Re}_D<0$ and ↑ for $\mathrm{Re}_D>0$) occur for all Reynolds numbers $-1.5\leq\mathrm{Re}_D\leq1.5$ from a convective instability of the basic flow and become absolutely unstable at higher Re_i. The experimentally determined absolute instability border (○) of the downstream propagating SPI (more precisely ↓ for $\mathrm{Re}_D<0$ and ↑ for $\mathrm{Re}_D>0$) is found to be in qualitative agreement with the results from linear stability analysis by Pinter *et al.* as shown in Fig. 4(a). The critical Reynolds numbers are obtained from experimental bifurcation diagrams like the one shown in Fig. 3(a).

In the experiments the convective instability border is shifted generally towards higher Re_i compared with the linear stability analysis of infinite systems due to the finite spatial extent [25]. For reasons of clarity we have omitted the experimental convective instability border in the stability diagram shown in Fig. 4(a).

Upstream propagating SPI (↑ for $\mathrm{Re}_D<0$ and ↓ for $\mathrm{Re}_D>0$) are observed for all Reynolds numbers between $-1.5\leq\mathrm{Re}_D\leq1.5$ but these flow states are stable only at a finite distance from the primary critical Re_i of the basic flow. The experimentally determined lower instability border of upstream propagating SPI is depicted in Fig. 4(b) (●). It is determined by a quasistatistical decrease of Re_i towards the critical Reynolds number Re_{c3} as demonstrated for $\mathrm{Re}_D=-1.5$ in Fig. 3(a). Upstream propagating SPI↓ are in the absolute unstable regime since no (large) fluctuations in amplitude and oscillation frequency can be found neither in time series nor in the power spectrum. A comparison with results from linear stability analysis, shown in Fig. 4, reveal that upstream propagating SPI are stable in the experiments even below their numerically calculated convective instability border. This provides experimental evidence that a secondary subcritical Hopf bifurcation towards upstream propagating SPI occurs from the (unstable) basic flow. Such a subcritical Hopf bifurcation is not covered by the nondegenerate model as shown in Eqs. (1) and (2) but only by a model of degenerate Hopf bifurcation with broken reflection symmetry [17]. Furthermore, the observation indicates that the observed flow states are always absolutely unstable since no convectively unstable regime of upstream propagating SPI has been found.

In general it can be seen from Fig. 4 that all experimentally determined instability lines and the numerically calculated absolute instability line merge smoothly at $\mathrm{Re}_D=0$, i.e., the case of closed Taylor-Couette flow. Here, the critical Re_i of both SPI↓ and SPI↑ are identical (apart from small deviations due to tiny imperfections in the apparatus) and convective instabilities do not occur. Note that the small difference in the numerical values of convective and absolute instabilities at $\mathrm{Re}_D=0$ is for numerical reasons [24]. The experimentally determined bifurcation structure is in qualitative agreement with predictions from theory and gives rise to the conclusion that an additional through-flow can be modeled by symmetry breaking imperfection terms added to the normal form of a Hopf bifurcation with O(2)-symmetry as presented for the nondegenerate case in Eqs. (1) and (2).

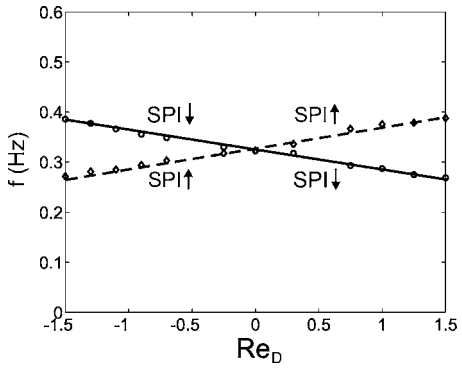

FIG. 5. Oscillation frequency f of SPI↑ (○) and SPI↓ (◇) measured at $\mathrm{Re}_o=-100.0$ and $\mathrm{Re}_i=109.0$: In the presence of an axial mean flow the frequency f of the primary downstream (secondary upstream) propagating SPI is increased (decreased) from the frequency at $\mathrm{Re}_D=0$. The frequency shift of both SPI↑ and SPI↓ depends linearly on Re_D.

Further evidence for this conclusion results from measurements of the dependence of the oscillation frequency on Re_D as presented in Fig. 5. Since the oscillation frequencies are found to be almost independent from Re_i close to the bifurcation, measurements on the dependence on Re_D were performed at $\mathrm{Re}_o=-100$ and $\mathrm{Re}_i=109$. The results are shown in Fig. 5. It can be seen that the oscillation frequency of downstream propagating SPI (↓ for $\mathrm{Re}_D<0$ and ↑ for $\mathrm{Re}_D>0$) is always shifted towards higher frequencies compared to those measured at $\mathrm{Re}_D=0$, i.e., the closed flow. On the other hand, upstream propagating SPI (↑ for $\mathrm{Re}_D<0$ and ↓ for $\mathrm{Re}_D>0$) always have a lower frequency. It is of particular interest that the dependence of the oscillation frequency of both SPI↓and SPI↑ on Re_D is almost linear but with opposite slope and has identical values for $\mathrm{Re}_D=0$. Such a behavior is predicted by theory of Hopf bifurcation with broken reflection symmetry [17] and by a model of Taylor-Couette flow with an axial through-flow [19].

D. Quasiperiodic flow

Models of imperfect bifurcations show generally more complicated dynamics and bifurcation structures than models of the corresponding symmetric bifurcation [16]. In particular symmetry breaking imperfections can be responsible for new dynamics, such as, e.g., modulated waves or chaos, that have no counterpart in the symmetric case. The theory of O(2)-symmetric Hopf bifurcation with broken reflection symmetry predicts a quasiperiodic state that results from a superposition of traveling waves having different amplitudes and frequencies [17]. Such a quasiperiodic flow has also

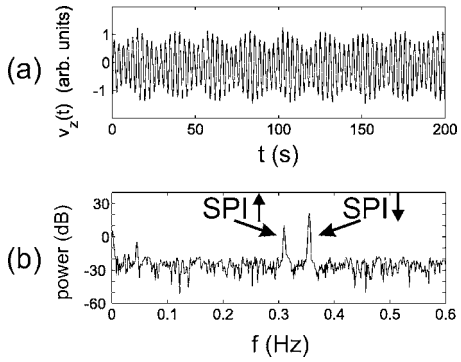

FIG. 6. Transient quasiperiodic flow observed at transition from up to downstream propagating SPI: (a) Time series representing transient quasiperiodic flow at $\mathrm{Re}_{(i,o,D)}=(107.0,-100.0,-0.9)$. (b) Two fundamental peaks corresponding to SPI↑ and SPI↓ in power spectrum from time series (a).

been predicted in a model of Taylor-Couette flow with an additional through-flow [19]. In theory the quasiperiodic flow state can appear from a secondary Hopf bifurcation of the upstream propagating traveling wave, i.e., spiral vortices (SPI) in the case of spiral Poiseuille flow.

In addition to that we found evidence for the existence of such a quasiperiodic flow in the spiral Poiseuille flow experiment. In Fig. 6(a), a time series of the axial velocity component v_z recorded at $\mathrm{Re}_{(i,o,D)}=(107.0,-100,-0.9)$ is depicted. At slightly larger Re_i the upstream propagating SPI↑ is stable. But when the Reynolds number is decreased towards $\mathrm{Re}_i=107.0$ this periodic flow becomes unstable and a quasiperiodic flow appears. In the power spectrum from the time series (a) which is depicted in Fig. 6(b) two fundamental peaks are observed. Both peaks can be identified as the oscillation frequencies of SPI↑ and SPI↓. The quasiperiodic flow is therefore characterized by a superposition of upstream and downstream propagating SPI, which is verified by flow visualization. The quasiperiodic flow exists in the experiments only as a transient of some minutes. A part of the time series is plotted in Fig. 6(a). A transition from this quasiperiodic flow towards the primary downstream propagating SPI↓ always occurs but after a (long) time.

IV. CONCLUSIONS

We have examined the effect of an imposed axial through-flow on bifurcation structure of spiral vortices in counter-rotating Taylor-Couette flow, i.e., in spiral Poiseuille flow. Our work demonstrates that the resulting bifurcation structure in a sufficiently long spiral Poiseuille flow experiment can be understood in terms of O(2)-symmetric Hopf bifurcation with broken reflection symmetry.

We have observed that downstream propagating spiral vortices appear always as a primary state from a Hopf bifurcation of the basic flow. This oscillatory regime splits up into a convective and an absolute unstable regime. The border of the absolute regime is found to be in quantitative agreement with recent numerical results from [24]. Upstream propagating spiral vortices also exist as finite-amplitude solutions but are observed only above a critical Re_i which has a finite distance to the primary Hopf bifurcation. This flow state is found to lose stability to a (transient) quasiperiodic flow which results from a superposition of SPI↑ and SPI↓. The observed bifurcation structure is found to be symmetric with respect to Re_D and merges towards the symmetric case at $\mathrm{Re}_D=0$. In the theory of Hopf bifurcation with broken reflection symmetry the influence of the finite length of an experimental system, the existence of inflow and outflow boundaries, as well as the appearance of convective instabilities are not considered. However, our experimental results provide evidence that the effect of an imposed axial flow on the bifurcation structure of spiral Poiseuille flow can be modeled by a symmetry breaking imperfection in accordance with theory for sufficiently long systems. The Reynolds number Re_D corresponds to the unfolding parameter of the imperfection in the normal form.

Thus the theory is robust and appropriate to describe effects of an imposed external flow on Hopf bifurcation with O(2)-symmetry in fluid flow experiments.

ACKNOWLEDGMENTS

We thank Wolfgang Schumann and Heinz Horak for the technical support. The authors acknowledge support from the "Deutsche Forschungsgemeinschaft." (J.L. and G.P.: Research Grant No. PF 210/10-1). We thank A. Pinter, C. Hoffmann, and M. Lücke for providing the numerical data published in [24].

[1] J. Guckenheimer and P. Holmes, *Nonlinear Oscillations, Dynamical Systems, and Bifurcations of Vector Fields* (Springer, New York, 1983), Vol. 42.

[2] T. Mullin, *The Nature of Chaos* (Clarendon Press, Oxford, 1993); H. L. Swinney and J. P. Gollub, *Hydrodynamic Instabilities and the Transition to Turbulence* (Springer, Berlin, 1981), Vol. 45; M. C. Cross and P. C. Hohenberg, Rev. Mod. Phys. **65**, 851 (1993).

[3] M. C. Cross, Phys. Rev. Lett. **57**, 2935 (1986); P. Kolodner, A. Passner, C. M. Surko, and R. W. Walden, *ibid.* **56**, 2621 (1986); V. Steinberg, J. Fineberg, E. Moses, and I. Rehberg, Physica D **37**, 359 (1986); W. Barten, M. Lücke, M. Kamps, and R. Schmitz, Phys. Rev. E **51**, 5636 (1995).

[4] P. C. Matthews and A. M. Rucklidge, Proc. R. Soc. London, Ser. A **441**, 649 (1993).

[5] F. Caton, B. Janiaud, and E. J. Hopfinger, Phys. Rev. Lett. **82**, 4647 (1999).

[6] P. Chossat and G. Iooss, *The Taylor-Couette Problem* (Springer, New York, 1994); R. Tagg, Nonlinear Sci. Today **4**, 2 (1994); *Physics of Rotating Fluids*, edited by C. Egbers and G. Pfister (Springer, Berlin, 2000).

[7] M. Golubitsky and I. Stewart, SIAM J. Math. Anal. **17**, 249

(1986); M. Golubitsky and W. F. Langford, Physica D **32**, 362 (1988).
[8] E. R. Krueger, A. Gross, and R. C. Di Prima, J. Fluid Mech. **24**, 521 (1966).
[9] H. A. Snyder, Phys. Fluids **11**, 728 (1968).
[10] C. D. Andereck, S. S. Lui, and H. L. Swinney, J. Fluid Mech. **164**, 155 (1986).
[11] W. F. Langford, R. Tagg, E. J. Kostelich, H. L. Swinney, and M. Golubitsky, Phys. Fluids **31**, 776 (1987).
[12] R. Tagg, W. S. Edwards, H. L. Swinney, and P. S. Marcus, Phys. Rev. A **39**, 3734 (1989).
[13] R. Tagg, W. S. Edwards, and H. L. Swinney, Phys. Rev. A **42**, 831 (1990); W. S. Edwards, R. P. Tagg, B. C. Dornblaser, H. L. Swinney, and L. S. Tuckerman, Eur. J. Mech. B/Fluids **10**, 205 (1991); J. Sanchez, D. Crespo, and F. Marques, Appl. Sci. Res. **51**, 55 (1993); O. Czarny, E. Serre, P. Bontoux, and R. M. Lueptow, Theor. Comput. Fluid Dyn. **16**, 5 (2002).
[14] J. Langenberg, G. Pfister, and J. Abshagen, Phys. Rev. E **68**, 056308 (2003); Phys. Fluids **16**, 2757 (2004); Phys. Rev. E **70**, 046209 (2004).
[15] E. Knobloch and G. Dangelmayr, Nonlinearity **4**, 399 (1991); A. S. Landsberg and E. Knobloch, Phys. Rev. E **53**, 3579 (1996); E. Knobloch and R. Pierce, in *Ordered and Turbulent Patterns in Taylor-Couette Flow*, edited by C. D. Andereck and F. Hayot, NATO Advanced Studies Institute, Series B: Physics (Plenum, New York, 1992), Vol. 297, p. 83.
[16] M. Golubitsky, I. Stewart, and D. G. Schaeffer, *Singularities and Groups in Bifurcation Theory: Vol. I*, no. 51 (Springer, New York, 1985); *Singularities and Groups in Bifurcation Theory: Vol. II*, no. 69 (Springer, New York, 1988); J. D. Crawford and E. Knobloch, Annu. Rev. Fluid Mech. **65**, 851 (1993).
[17] J. D. Crawford and E. Knobloch, Nonlinearity **1**, 617 (1988).
[18] S. A. van Gils and J. Mallet-Paret, Proc. - R. Soc. Edinburgh, Sect. A: Math. **104**, 279 (1986).
[19] R. Raffaï and P. Laure, Eur. J. Mech. B/Fluids **12**, 277 (1993).
[20] P. Huerre and P. A. Monkewitz, Annu. Rev. Fluid Mech. **22**, 473 (1990).
[21] S. M. Tobias, M. R. E. Proctor, and E. Knobloch, Physica D **113**, 43 (1998); J. M. Chomaz and A. Couairon, Phys. Fluids **11**, 2977 (1999).
[22] K. L. Babcock, G. Ahlers, and D. S. Cannell, Phys. Rev. Lett. **67**, 3388 (1991); Phys. Rev. E **50**, 3670 (1994); A. Tsameret and V. Steinberg, Phys. Rev. Lett. **67**, 3392 (1991); Phys. Rev. E **49**, 1291 (1994); R. M. Lueptow, A. Doctor, and M. Kyungyoon, Phys. Fluids A **4**, 2446 (1992).
[23] A. Recktenwald, M. Lücke, and H. W. Müller, Phys. Rev. E **48**, 4444 (1993); P. Büchel, M. Lücke, D. Roth, and R. Schmitz, *ibid.* **53**, 4764 (1996); A. Szprynger and M. Lücke, *ibid.* **67**, 046301 (2003).
[24] A. Pinter, M. Lücke, and C. Hoffmann, Phys. Rev. E **67**, 026318 (2003); C. Hoffmann, M. Lücke, and A. Pinter, *ibid.* **69**, 056309 (2004).
[25] J. Langenberg, M. Heise, G. Pfister, and J. Abshagen, Theor. Comput. Fluid Dyn. **18**, 97 (2004).
[26] K. L. Babcock, G. Ahlers, and D. S. Cannell, Phys. Rev. E **50**, 3670 (1994).